THE ASTROPHYSICAL JOURNAL, 377:L53–L56, 1991 August 10


# FIRST RESULTS FROM THE GODDARD HIGH-RESOLUTION SPECTROGRAPH: ELEMENT ABUNDANCES AS A FUNCTION OF VELOCITY IN THE NEUTRAL GAS TOWARD $\xi$ PERSEI

BLAIR D. SAVAGE,[1] JASON A. CARDELLI,[1] FREDERICK C. BRUHWEILER,[2] ANDREW M. SMITH,[3]
DENNIS C. EBBETS,[4] AND KENNETH R. SEMBACH[1]

*Received 1991 March 29; accepted 1991 April 20*

## ABSTRACT

Observations of ultraviolet interstellar absorption lines toward $\xi$ Persei (HD 24912) obtained with the echelle mode of the Goddard High-Resolution Spectrograph (GHRS) aboard the *Hubble Space Telescope* at a resolution of 3.5 km s$^{-1}$ are presented. The data for O I, C II, Mg II, S II, Fe II, Si II, Mn II, and Zn II are converted into representations of apparent column density per unit velocity, $N_a(v)$, over the velocity range from $-30$ to $+40$ km s$^{-1}$. The profiles for ions that are the dominant state of ionization in neutral clouds permit a study of the variation of element abundance with velocity caused by changes in the gas phase depletion in the different absorbing regions situated toward $\xi$ Per. In the denser portions of the diffuse clouds with $v \sim +5$ to 15 km s$^{-1}$, heavy element depletions are very large. However, in absorbing components near $-5$ and $+25$ km s$^{-1}$, the depletions are less severe, with a nearly solar gas phase abundance ratio being found for the gas in the $+25$ km s$^{-1}$ component. The measurements confirm that the GHRS is well suited for diagnostic spectroscopy of interstellar gas.

*Subject headings:* interstellar: abundances — interstellar: matter — stars: individual ($\xi$ Persei) — ultraviolet: spectra

## 1. INTRODUCTION

The star $\xi$ Persei (HD 24912) is an O7.5 III star in the direction $l = 160\overset{\circ}{.}4$ and $b = -13\overset{\circ}{.}1$ at an estimated spectroscopic distance of 540 pc. The large $v \sin i$ (216 km s$^{-1}$; Uesugi & Fukuda 1970) and heliocentric radial velocity ($+70$ km s$^{-1}$; Wilson & Joy 1950), make $\xi$ Per well suited for studies of narrow interstellar absorption lines. The gas toward $\xi$ Per has been the subject of a number of previous investigations (see Gomez-Gonzalez & Lequeux 1975 and references therein).

The $\xi$ Per sight line provides an excellent opportunity to determine the diagnostic powers of the Goddard High-Resolution Spectrograph (GHRS) aboard the *Hubble Space Telescope* (*HST*), which provides astronomers with the possibility of obtaining ultraviolet spectra with very high spectral resolution [$\lambda/\Delta\lambda$ from $7.8 \times 10^4$ to $9.4 \times 10^4$ or FWHM ($v$) from 3.8 to 3.2 km s$^{-1}$] and high signal-to-noise ratio ($>200/1$).

## 2. OBSERVATIONS

Ultraviolet observations of interstellar absorption toward $\xi$ Per were obtained by the GHRS in 1990 October and 1991 January. The measurements were obtained with the GHRS operating in the echelle modes with the light of $\xi$ Per placed in the small ($0\overset{''}{.}25 \times 0\overset{''}{.}25$) entrance aperture. For details about the GHRS, its preflight performance characteristics, and its modes of operation, see Duncan & Ebbets (1989). Most of the interstellar line measurements were obtained using scan sequence 6 (FP-SPLIT) and four position comb-addition. Observations were obtained at 26 different setup wavelengths with each observation providing approximately 5–10 Å coverage of the ultraviolet spectrum. The total integration time for each spectral region observed was typically 3–6 minutes. The signal-to-noise ratio achieved in the reduced data ranges from 15 to 100 depending on the wavelength and the accuracy of centering the star in the small aperture.

The data were processed using the techniques described by Cardelli et al. (1991). These techniques properly remove the interorder echelle scattered light background and permit the precise alignment of the FP-SPLIT subexposures when the individual subexposures are combined into a single spectrum.

Figure 1 illustrates a full GHRS Digicon 500 channel spectrum of $\xi$ Per at two samples per diode in the wavelength region from 1298 to 1306 Å. The interstellar lines seen are listed in the figure legend. Note that the strongly saturated O I line has broad radiation damping wings. Lines arising in Earth's atmosphere include O I $\lambda$1302.169 and O I* $\lambda$1304.858. The motion of the satellite relative to Earth at the time of observation Doppler-shifted these lines away from the interstellar lines. The atmospheric lines permit a precise wavelength calibration of the interstellar lines shown in the figure. Data like those shown in Figure 1 have been used to produce the interstellar absorption line profiles illustrated in Figure 2. Information about the lines illustrated in Figure 2 and other absorption lines considered in this paper is found in Table 1.

The absorption-line wavelengths have been adjusted using the wavelength "bootstrap technique" discussed by Cardelli et al. (1991). This technique adjusts for errors of approximately $\pm 2$ km s$^{-1}$ (1 $\sigma$) produced by a combination of imprecision in the GHRS grating carousel positioning, magnetic effects in the Digicon produced by Earth's magnetic field, and uncertainties in the spectrograph dispersion constants.

## 3. AN OVERVIEW OF ABSORPTION-LINE VELOCITIES

The setup wavelengths provided for the detection of interstellar absorption lines from the following ions: C I, C I*,

[1] Washburn Observatory, University of Wisconsin, 475 North Charter Street, Madison, WI 53706.
[2] Department of Physics, Catholic University of America, Washington, DC 20064.
[3] Laboratory for Astronomy and Solar Physics, NASA/Goddard Space Flight Center, Greenbelt, MD 20771.
[4] Ball Aerospace Systems, PO Box 1062, Boulder, CO 80306.

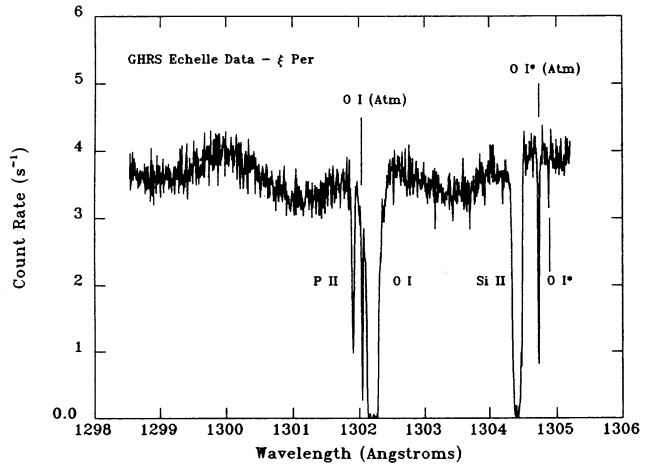


FIG. 1.—The full 500 channel GHRS Digicon spectrum of $\xi$ Per obtained with the spectrograph operating in echelle order 43. Net count rate is plotted vs. heliocentric vacuum wavelength in Å. Interstellar lines recorded include P II $\lambda$1301.87, O I $\lambda$1302.17, Si II $\lambda$1304.37 and O I* $\lambda$1304.86. Note the damping wings on the strong interstellar line of O I $\lambda$1302.17. Earth atmospheric lines of O I $\lambda$1302.17 and O I* $\lambda$1304.86 permit accurate wavelength calibration of the interstellar lines recorded in the spectrum. The S/N in this small aperture spectrum is about 25.

C I**, C II, C II*, C IV, O I, O I*, Mg I, Mg II, Al III, Si II, P II, S I, S II, S III, Cl I, Cr II, Mn II, Fe II, Ni II, Cu II, Zn II, and the CO molecule.

The velocity structure of the absorption toward $\xi$ Per is as follows:

TABLE 1

INTERSTELLAR LINES ANALYZED

| Mode/Order[a] | Species | $\lambda$ (Å)[b] | log [$f\lambda$ (Å)][c] |
|---|---|---|---|
| A/42 | C II | 1334.532 | 2.232 |
| B/24 | C II] | 2325.403 | −3.982 |
| A/43 | O I | 1302.169 | 1.805 |
| A/41 | O I | 1355.598 | −2.772 |
| A/45 | Mg II | 1239.925 | −0.479 |
| A/45 | Mg II | 1240.395 | −0.780 |
| B/20 | Mg II | 2803.531 | 2.933 |
| B/20 | Mg II | 2796.352 | 3.234 |
| B/31 | Si II | 1808.013 | 1.000 |
| A/43 | Si II | 1304.370 | 2.284 |
| A/47 | Si II | 1190.416 | 2.474 |
| A/47 | Si II | 1193.290 | 2.775 |
| A/45 | S II | 1250.584 | 0.834 |
| A/45 | S II | 1253.811 | 1.135 |
| B/24 | Mn II | 2305.714 | 0.456 |
| B/22 | Mn II | 2606.462 | 2.701 |
| B/25 | Fe II | 2249.877 | 0.752 |
| B/25 | Fe II | 2260.780 | 0.924 |
| B/24 | Fe II | 2374.461 | 1.826[d] |
| B/23 | Fe II | 2382.765 | 2.855 |
| B/22 | Fe II | 2600.173 | 2.765 |
| B/28 | Zn II | 2026.136 | 3.018 |
| B/27 | Zn II | 2062.664 | 2.717 |

[a] Echelle mode A or B and order number.
[b] Vacuum wavelength from Morton 1991.
[c] log [$f\lambda$(Å)] from Morton 1991.
[d] Analysis of the Fe II apparent column density profiles discussed in the text indicates that the log ($f\lambda$) value of the $\lambda$2374 line must be corrected by +0.15 dex to be consistent with the results for the other lines. We therefore used log ($f\lambda$) = 1.976 in our analysis.

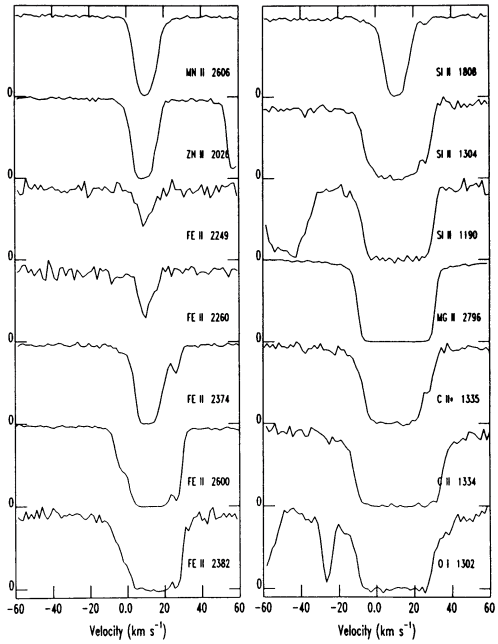


FIG. 2.—Relative intensity vs. heliocentric velocity for a sample of interstellar lines in the spectrum of $\xi$ Per. The zero-level of each line is indicated on the vertical axis in each panel. Information about the lines shown is provided in Table 1. For Si II and Fe II the availability of absorption lines with a wide range of oscillator strength permits an evaluation of the nature of the absorption over a wide range of velocity. The low column density absorption components near −5 and +25 km s$^{-1}$ are readily apparent in the sequence of Fe II $\lambda\lambda$2374.46, 2382.77, 2600.17 profiles illustrated. In several cases, more than one absorbing species appears on the short portion of the ultraviolet spectrum illustrated. Zn II $\lambda$2026.14 where Mg I $\lambda$2026.48 appears for $v > 50$ km s$^{-1}$; Si II $\lambda$1190.42 where S III $\lambda$1190.21 appears for $v < -30$ km s$^{-1}$; and O I $\lambda$1302.17 where terrestrial O I $\lambda$1302.17 appears near $v = -27$ km s$^{-1}$ and P II $\lambda$1301.87 appears for $v < -50$ km s$^{-1}$.

1. The diffuse clouds which are traced by the weaker absorption lines of neutral and once ionized atoms absorb between +5 and +15 km s$^{-1}$ (see Fig. 2). The atomic abundances in these clouds are discussed in the GHRS paper by Cardelli et al. (1991). The molecular and neutral gas phase conditions in these clouds are the subject of the GHRS paper by Smith et al. (1991).

2. Ionized gas absorption is traced by the GHRS measures of Al III, S III, Si IV, and C IV. The Al III and S III lines indicate broad absorption extending from −20 to +20 km s$^{-1}$. The lines of Si IV and C IV also absorb in this velocity range although their profile shapes are considerably different than those for Al III and S III. N V $\lambda$1238 absorption was not detected in the low S/N spectrum obtained by the GHRS at 1238 Å.

3. The strong ultraviolet lines of species such as Fe II, Si II, O I, and C II reveal additional absorption at velocities different from those of the diffuse clouds. In particular, the lines of Fe II and Si II reveal components near −5 km s$^{-1}$ and +25 km s$^{-1}$ (see Fig. 2). These strong UV lines permit the detection of low column density gas with gas phase abundances very different from those found in the diffuse clouds toward $\xi$ Per.

## 4. ELEMENT ABUNDANCES AS A FUNCTION OF VELOCITY

The 3.5 km s$^{-1}$ resolution provided by the echelle mode of the GHRS means that in many cases the absorption-line measurements obtained by the spectrograph will be either fully resolved or close to being fully resolved. When an absorption

line is fully resolved, the observed optical depth of absorption is given by

$$\tau(v) = \ln\left[\frac{I_0(v)}{I_{\rm obs}(v)}\right] = \frac{\pi e^2}{m_e c} f\lambda N(v)$$
$$= 2.654 \times 10^{-15} f\lambda N(v)\,, \quad (1)$$

where $I_0(v)$ and $I_{\rm obs}(v)$ are the continuum intensity and observed intensity, respectively, $N(v)$ is the column density per unit velocity in atoms cm$^{-2}$ (km s$^{-1}$)$^{-1}$, $f$ is the oscillator strength of the line, and $\lambda$ is the wavelength in Å. When an absorption line is not fully resolved, we refer to the optical depth as derived above as the apparent optical depth, $\tau_a(v)$, and the corresponding column density as the apparent column density, $N_a(v)$.

The high-resolution absorption-line data can be converted into measures of $N_a(v)$ extending over a large range of $v$ by combining the absorption measurements for lines of different strength. The weak lines will determine $N_a(v)$ at velocities where the column density per unit velocity is large while strong lines will determine $N_a(v)$ at velocities where it is small. If a given species has a number of lines, it is possible to construct a complete $N_a(v)$ profile and use the empirical information in the region of velocity overlap from one line to the next to infer the presence or absence of unresolved saturated structures in the derived profiles. The technique is applied to the absorption line data for Fe II in Figure 3*a*. When $N_a(v)$ profiles derived from lines differing in $f$ value by more than a factor of 2 agree in a region where they overlap in velocity, the work of Savage & Sembach (1991) has demonstrated that it is reasonable to assume that unresolved saturated structures are not influencing the values of $N_a(v)$. The good correspondence between the values of $N_a(v)$ derived from the different Fe II lines contributing to Figure 3*a* implies that the derived solid curve is a reliable representation of $N_a(v)$ for Fe II. In a similar fashion curves of $N_a(v)$ were derived for other species and are shown in Figures 3*b* and 3*c*.

The construction of $N_a(v)$ curves from the GHRS data permits a study of how different elements change gas phase abundances as a function of velocity. The power of the technique is revealed in Figures 3*b* and 3*c* where normalized $N_a(v)$ profiles are plotted for a number of species representing the dominant state of ionization in neutral hydrogen regions. In Figure 3*b* all the individual $N_a(v)$ profiles are plotted in the

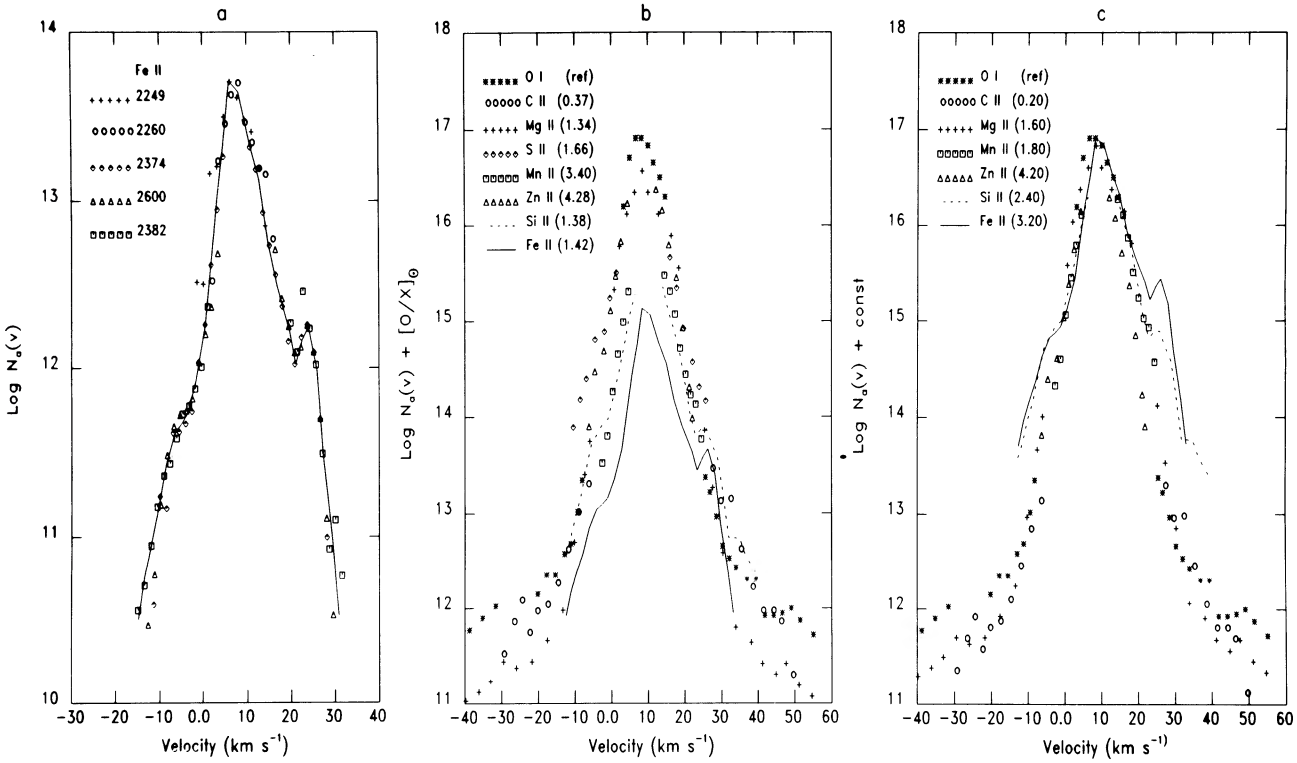


FIG. 3.—In (*a*) the Fe II ultraviolet absorption-line measurements for ξ Per have been converted into logarithmic plots of apparent column density as a function of heliocentric velocity, log $N_a(v)$ [atoms cm$^{-2}$ (km s$^{-1}$)] using eq. (1) and the procedures discussed in Savage & Sembach (1991). Saturated regions of the stronger Fe II lines are not plotted. The components near $v = -5$ and $+25$ km s$^{-1}$ are apparent in the log $N_a(v)$ profile for Fe II. The Fe II λ2382 data point at $+22$ km s$^{-1}$ is a low S/N measurement.

In (*b*) we display curves of log $N_a(v)$ + $[O/X]_\odot$ for O I, C II, Mg II, Si II, Fe II, S II, Mn II, and Zn II, with $[O/X]_\odot$ listed in the figure legend. The value of $[O/X]_\odot$ for a given element was taken to be the logarithmic abundance difference for that element compared to oxygen and was obtained from the solar system abundances of Morton (1991). Thus, all the curves are corrected for solar abundance differences and are referenced to oxygen, a species that is only slightly depleted in diffuse interstellar clouds. At velocities where the curves for two species overlap, the two species therefore have solar abundance ratios. The large vertical separation of some of the curves at velocities corresponding to those of the diffuse clouds ($v \sim +5$ to $+15$ km s$^{-1}$) is caused by the depletion of the various elements into interstellar dust. Note that Lorentzian wings appear on the profiles for species with very strong lines (i.e., C II, O I, and Mg II).

In (*c*) the curves from (*b*) have been adjusted vertically and replotted to make them coincide over the heliocentric velocity range from $\sim +5$ to $+15$ km s$^{-1}$ which represents the velocity range where the denser portions of the diffuse clouds toward ξ Per absorb. With this normalized set of curves, it is possible to view how the gas phase abundances of various species change from the denser absorbing regions to the lower column density medium toward ξ Per. The normalization constants required to produce the figure are listed in the figure legend.

column density system of the lightly depleted O I atom after correcting for the solar element to element abundances listed in Morton (1991). A $N_a(v)$ profile lying below that for O I in Figure 3*b* indicates that the species is depleted from the gas phase. For example, the curve for Fe II lies approximately 2.0 dex below that of O I for $v \sim +5$ to $+15$ km s$^{-1}$ because Fe in diffuse clouds is depleted into interstellar dust. At velocities where the curves of Figure 3*b* overlap, the relative abundances of the absorbing species are solar.

In Figure 3*c* the curves illustrated in Figure 3*b* have been vertically adjusted to coincide near line center, ($v \sim +5$ to $+15$ km s$^{-1}$). This normalization permits an assessment of how the absorption profiles for the different atoms change in going from the strongly absorbing diffuse clouds to the lower column density medium at velocities away from the peak absorption. From an inspection of Figures 3*b* and 3*c* we note the following: Near the maximum of absorption, the ordering of the vertical positioning of the curves shown in Figure 3*b* is indicative of the different levels of depletion from one element to the next in the diffuse clouds. However, note that in a number of cases the weakest lines are too strong to provide useful information at the peak of absorption. Lorentzian damping wings are apparent in the profiles for O I, C II, and Mg II for $v > 30$ km s$^{-1}$ and $v < -10$ km s$^{-1}$. The existence of damping wings permits the derivation of reliable total column densities for O I, C II, and Mg II (see (Cardelli et al. 1991). In Figure 3*c*, at $v \sim -5$ km s$^{-1}$ and $v \sim +25$ km s$^{-1}$, the curves for Fe II and Si II lie substantially above the level established by the curves for S II, Zn II, Mn II, Mg II, O I, and C II. This indicates a large gas phase abundance increase for Si and Fe in the low column density medium producing the two components. In the component near $-5$ km s$^{-1}$ the enhancement in log $N_a(v)$ for Si II and Fe II compared to the level established by Zn II and Mn II is approximately 0.3 dex. In the component near $+25$ km s$^{-1}$ Fe II is enhanced by about 2.0 dex and Si II is enhanced by about 1.5 dex, compared to O I and Zn II in Figure 3*c*. In Figure 3*b*, we see that the Fe II and Si II abundance enhancements are the result of having Fe II and Si II gas phase abundances closer to solar in the $-5$ and $+25$ km s$^{-1}$ components than in the more strongly absorbing medium. In the component at $-5$ km s$^{-1}$, the curves of Figure 3*b* imply that the Si II and Fe II depletions are approximately 1.0 and 1.8 dex, respectively, when referenced to S II, an element that is lightly depleted. In the component at $+25$ km s$^{-1}$, the curves of Figure 3*b* reveal that Si II and Fe II have relative gas phase abundances within 0.3 dex of that found in the Sun. This similarity may also extend to the other elements whose curves pass near those for Si II and Fe II. The amount of gas in the $+25$ km s$^{-1}$ component can be estimated from plots of log $N_a(v)$. The profiles for the component are approximately fitted with an instrumentally broadened line having $b = 2$ km s$^{-1}$ and total column densities log $N$(Si II) = 13.28 and log $N$(Fe II) = 12.92. Assuming a solar gas phase abundance for Si, the corresponding column density of neutral hydrogen is log $N$(H I) = 17.78.

## 5. DISCUSSION

The GHRS data analyzed here represent the first high-resolution view of the full velocity-dependent nature of absorption for a number of abundant atoms along an interstellar sight line (see Figs. 3*b* and 3*c*). The curves of log $N_a(v)$ shown in Figure 3*b*, which are adjusted for solar abundance differences, allow an evaluation of the large changes in the gas phase abundances of various elements as a function of velocity toward $\xi$ Per. Of the elements plotted, Fe is the most depleted in the low-velocity diffuse cloud (Cardelli et al. 1991), and thus the curve for Fe II lies about 2 dex below that for O I in the velocity range from $+5$ to $+15$ km s$^{-1}$. However, at other velocities the amount of Fe II and Si II found in the gas is enhanced. At $+25$ km s$^{-1}$, the nearly solar ratio found for Si II to Fe II suggests little depletion and the curves for many other elements seem to join up near $+25$ km s$^{-1}$ in Figure 3*b*. This suggests nearly solar abundance ratios for C II, O I, Mg II, Mn II, and Zn II as well. Evidently in the lower column density medium the heavily depleted elements are returned to the gas phase by a process that has converted dust into gas with nearly complete conversion in the $+25$ km s$^{-1}$ component and partial conversion in the $-5$ km s$^{-1}$ component.

Optical absorption line data for $\xi$ Per shown in Stokes (1976) reveal a weak Ca II feature in the velocity range $+25$ to $+32$ km s$^{-1}$ with log $N$(Ca II) = 11.15 (Stokes 1976, Table 3, p. 124, but note that the $\xi$ was inadvertantly listed as $\zeta$). This feature is not seen in Na I or Ti II. Its absence in the normally stronger Na I line implies that the feature is an example of an interstellar component with an anomalously large value of $N$(Ca II)/$N$(Na I). Such components were first studied by Routly & Spitzer (1952). The extension of these studies to other elements through *Copernicus* satellite observations of two stars is found in Shull & York (1977). For a review see Jenkins (1987). The processing of interstellar dust with the subsequent liberation of elements to the gas phase appears to be the most likely explanation for the large gas phase abundance variations found in these first GHRS observations of $\xi$ Per. It is apparent that the GHRS will make major contributions to studies of the relationship between gas and dust in interstellar space and the processing of dust that occurs in intermediate and high velocity interstellar clouds.

We thank the many dedicated people involved in the GHRS project for their efforts in producing a very high quality ultraviolet spectrograph and in particular we want to acknowledge John Brandt, the Principal Investigator, and Sally Heap, the Co–Principal Investigator for the instrument. The data processing performed as part of this research used the computing facilities of the Midwest Astronomical Data Reduction and Analysis Facility. Data handling support from Marilyn Meade and Brian Babler is appreciated. J. A. C. and B. D. S. acknowledge support for their involvement in GHRS through NASA contract NAS5-29638. D. C. E. acknowledges support through NASA contract NAS5-26000.

## REFERENCES

Cardelli, J. A., Savage, B. D., Bruhweiler, F. C., Smith, A. M., Ebbets, D. C., Sembach, K. R., & Sofia, U. J. 1991, ApJ, in press
Duncan, D. K., & Ebbets, D. C. 1989, Goddard High Resolution Spectrograph Instrument Handbook, Space Telescope Science Institute
Gomez-Gonzalez, J., & Lequeux, J. 1975, A&A, 38, 29
Jenkins, E. B. 1987, in Interstellar Processes, ed. D. J. Hollenbach & H. A. Thronson, Jr. (Dordrecht: Reidel), 533
Morton, D. C. 1991, ApJS, in press
Routly, P. M., & Spitzer, L. 1952, ApJ, 115 227
Savage, B. D., & Sembach, K. R. 1991, ApJ, in press
Shull, J. M., & York, D. G. 1977, ApJ, 211, 803
Smith, A. M., Bruhweiler, F. C., Lambert, D. L., Savage, B. D., Cardelli, J. A., Ebbets, D. C., Lyu, C.-H., & Sheffer, Y. 1991, ApJ, submitted
Stokes, G. M. 1976, ApJS, 36, 115
Uesugi, A., & Fukuda, I. 1970, Contr. Inst. Ap. Kwasan Obs. Univ. Kyoto, 189
Wilson, R. E., & Joy, A. H. 1950, ApJ, 111, 221